International Journal of Energy Horizon 02 (2025) 70-79

International Journal of Energy Horizon

journal homepage: https://dergipark.org.tr/tr/pub/ijeh

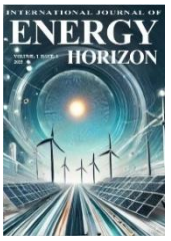

Research Article

Exergoeconomic evaluation of an S-CO_2 cycle coupled with a gas engine in a solid waste power plant

Alperen Tozlu[1,2], Marta Trninic[3], Emrah Özahi[4*]

[1] Bayburt University, Vocational School of Technical Sciences, Electricity and Energy, Bayburt, Türkiye
[2] Toraighyrov University, Faculty of Energetics, Heat and Power Engineering Department, Pavlodar, Kazakhstan
[3] The Academy of Applied Studies Polytechnic, Serbia
[4] Gaziantep University, Mechanical Engineering Department, Gaziantep, Türkiye
[1]ORCID No: 0000-0002-2610-5279
[3]ORCID No: 0000-0001-6916-6162
[4]ORCID No: 0000-0003-3940-9500

ARTICLE INFO

Article History:

Received:10 October 2025
Revised:6 November 2025
Accepted:15 November 2025
Available online:30 November 2025

Keywords:

S-CO_2
Thermo-economy
Optimization
Genetic Algorithm
Waste-to-energy

ABSTRACT

In this study, the exhaust waste heat recovery from a gas engine of a municipal solid waste power plant (MSWPP) in Bayburt city, Turkey, through the application of a supercritical carbon dioxide (S-CO_2) cycle was investigated. The plant with an installed power capacity of 1450 kW, can be possible to generate an additional 108.65 kW of power by integrating the S-CO_2 system, corresponding to approximately 7.5% extra power production. A thermodynamic model was developed using actual data of the plant, enabling accurate assessment of system performance. The energetic and exergetic efficiencies of the developed cycle were determined in terms of energy transfer and exergy destruction values. Exergoeconomic analyses were also carried out using the Specific Exergy Costing (SPECO) method, providing cost allocation and investment insights for the plant components. The results reveal that the coupling of S-CO_2 cycle increases both the energy and exergy efficiencies, while also improving the overall economic performance. Consequently, the proposed system offers a sustainable and effective solution for the recovery of waste heat in solid waste-based power generation stations.

1. INTRODUCTION

Gas turbine power plants present considerable potential as a complementary technology to conventional power generation facilities and internal combustion (IC) gas engine power plants. Although gas turbines gained prominence during the 1950s and 1970s, they were subsequently eclipsed by open-cycle gas turbines due to their superior efficiency and higher firing temperatures. However, recent advancements in working fluid technologies have renewed interest in closed-cycle gas turbines, which are now being investigated as alternatives for power conversion systems [1]. Fundamentally, a gas turbine system operates on Brayton cycle to generate mechanical power. Gas turbines are categorized into open cycle (air), closed cycle (air or another medium), and also semi-open cycle configurations. Additionally, closed-cycle gas turbines are distinguished by the type of thermal source and working fluid employed. In the literature, fossil fuels, nuclear, solar, and biomass have been considered as heat sources, while air is a working fluid, supercritical CO_2 (S-CO_2), helium, nitrogen and other noble gases. Exhaust gases released from gas turbines and diesel engines represent low-temperature waste heat sources that, when treated as renewable-type energy inputs, offer substantial potential for meeting global energy demand [1–7]. Power cycles utilizing S-CO_2 have been identified and developed as effective methods due to conversion of low grade heat into useful energy potential. Notably, a waste heat recovery unit coupled with an S-CO_2 power cycle (capable of generating 8 MW) entered the electricity market for the first time in 2014, marking a milestone in this field [8]. Moreover, S-CO_2 power cycle applications are found in systems where closed-cycle gas turbines are integrated at the back end and in high-temperature fuel cell systems (e.g., sodium and helium reactors) [1, 9–11]. For instance, Ahmadi et al. [12] developed an S-CO_2 power cycle utilizing a typical geothermal heat reservior and designed a natural-gas liquefaction system powered by the waste heat of this cycle. In their study, the exergy efficiency of 20.5% and an annual electricity cost of USD 263,592 were found. Similarly, Akbari and

*Corresponding author
E-mail address: alperentozlu@bayburt.edu.tr
journal homepage: https://dergipark.org.tr/tr/pub/ijeh

Mahmoudi [13] proposed an S-CO_2 power cycle in which the thermal difference of the intercooler was harnessed as the evaporator of an organic Rankine cycle (ORC), thereby improving thermodynamic efficiency in the overall system. In another study, Kim et al. [14] analyzed nine different closed gas turbine cycles coupled to S-CO_2 in another landfill-gas-fired gas turbine plant. Their findings revealed that the recuperator played a more decisive role than the intercooler in enhancing thermal efficiency and total power generation. Nami et al. [15] proposed combining the waste heat of an open gas turbine cycle with an S-CO_2 closed gas turbine cycle, and subsequently using the remaining waste heat in an ORC system. Wang and Dai [16] designed two separate gas turbines employing transcritical CO_2 (T-CO_2) as the working fluid and dual heat exchangers to assess waste heat from a helium reactor. There are also many other studies that were carried out in this respect [17-21].

In the related study, an effective model is proposed to utilize the waste heat from a municipal solid waste into energy power plant located in Bayburt, Turkey, an operational facility generating electricity, to recover energy based on actual plant operating data. The proposed model underwent thermodynamic and thermoeconomic analyses [22]. Within the developed framework, waste heat was utilized as a thermal source in an S-CO_2 gas turbine cycle, thereby augmenting the power output of the existing facility. The primary novelty of this work lies in its status as the first study to evaluate waste heat recovery from an operational municipal solid waste-to-energy plant in Bayburt, with the objective of enhancing the plant's electricity generation capacity. Consequently, thermodynamic and thermoeconomic analyses were conducted to derive technical and economic performance indicators that could serve as benchmarks for system improvements. Cost assessments were performed using the well-known specific exergy cost (SPECO) method, which is grounded in 2nd law of thermodynamics. The exergetic costs of streams, subsystem exergy-destruction costs, and investment and operation-maintenance expenses were determined using cost-balance equations developed for each subsystem. Compared to conventional economic analyses that overlook system irreversibilities, the proposed exergy-based cost analysis offers a more rational approach by accounting for exergy destruction costs. Therefore, the proposed model and its associated thermodynamic and thermoeconomic evaluations are anticipated to be highly beneficial and practical for waste-heat recovery utilization and for enhancing the management of existing systems.

2. MATERIAL AND METHODOLOGY

2.1. Description of the Proposed System

The Bayburt Municipal Solid Waste Power Plant (BMSWPP) has been established in order to manage the solid-waste generated by Bayburt and its neighboring municipalities. This facility possesses a power capacity of 1.45 MW, which is produced using a gas engine. In the related study, a recompression supercritical carbon dioxide (S-CO2) gas turbine cycle was utilized and integrated as a model to augment the electrical output of the existing system by utilizing the plant's exhaust gas. Exhaust gas from the plant exhibited the temperature of 431 °C, the pressure of 1 bar and the mass flow rate of 2.181 kg/s. The newly developed system comprises gas-turbine (GT), a gas-turbine heat-exchanger (GTHE), low-pressure compressor (LPC), high-pressure compressor (HPC), precooler (PRE), recuperator (REC) and intercooler (INT).” should be changed as ‘’The newly developed system comprises a gas-turbine (GT), a gas-turbine heat-exchanger (GTHE), a low-pressure compressor (LPC), a high-pressure compressor (HPC), a precooler (PRE), a recuperator (REC), and an intercooler (INT). The main reason for naming it the ‘gas turbine heat exchanger’ is that the overall system is integrated with a gas turbine, and the heat exchanger’s primary role is to utilize the gas turbine’s exhaust gas as the main thermal input to drive the S-CO_2 cycle. Figure 1 presents a schematic layout of the system. The re-compression S-CO2 gas turbine cycle has been based on definition of the inlet conditions for the system's low-pressure compressor. At the inlet state of the low-pressure compressor, the temperature and pressure of S-CO2 (Pcrit= 73.8 bar and Tcrit=30.98 °C) were set at 40 °C and 85 bar, respectively, which exceed the critical values. To establish a feasible power cycle model, the CO2 pressure was constrained to 85–229.5 bar [15]. The pressure ratio (PR) between the compressors was determined to be 2.5 based on the CO2 pressure. The heat exchangers’ effectiveness (εf_{HE}) and the compressors’ and gas turbine’s isentropic efficiencies (η_C, η_{GT} , respectively, , respectively) have been assumed to be 0.85, 0.85, and 0.92, respectively, as is commonly reported in the literature [21-22]. Furthermore, the study was carried out under the general assumptions of a steady state operation, neglecting kinetic and potential energy changes, disregarding pressure losses in pipes and heat exchangers and being saturated liquid of the working fluid at the exit of the precooler and intercooler.

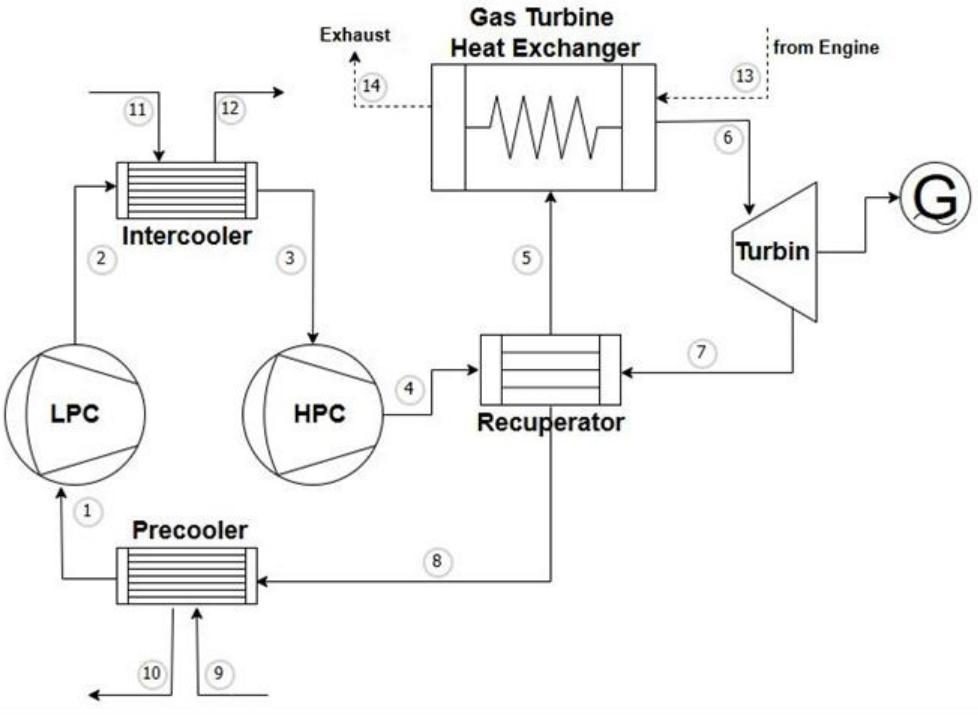

Figure 1. Schematic representation of the cycle

2.1. Thermodynamic And Thermoeconomic Analyses

By applying the related governing equations listed in Table 1, the heat transfer, work interaction, exergy destruction values, and exergy efficiencies of the subsystems were determined. In addition, the specific exergy of the flow and the corresponding exergy rate were found using the following relations [21-22];

$$\psi = (h - h_0) - T_0(s - s_0) \quad (1)$$

$$\dot{E}x = \dot{m}\psi \quad (2)$$

The energetic and exergetic efficiencies were determined using the following equations [21-22];

$$\eta = (\dot{W}_{GT} - (\dot{W}_{LPcomp} + \dot{W}_{HPcomp}))/\dot{m}_{exh}(h_{13} - h_{14}) \quad (3)$$

$$\varepsilon = (\dot{W}_{GT} - (\dot{W}_{LPcomp} + \dot{W}_{HPcomp}))/\dot{m}_{exh}(\psi_{13} - \psi_{14}) \quad (4)$$

Table 1. Schematic representation of the cycle

Gas Turbine Heat Exchanger	**Gas Turbine**
$\dot{m}_{13} = \dot{m}_{14} = \dot{m}_{exh}, \dot{m}_5 = \dot{m}_6 = \dot{m}_{CO_2}$	$\dot{m}_6 = \dot{m}_7 = \dot{m}_{CO_2}$
$\dot{m}_{exh}(h_{13} - h_{14}) = \dot{m}_{CO_2}(h_6 - h_5)$	$\dot{W}_{GT,a} = \dot{m}_{CO_2}(h_6 - h_7)$
$\dot{E}x_{D,GTHE} = \dot{m}_{exh}(\psi_{13} - \psi_{14}) - \dot{m}_{CO_2}(\psi_6 - \psi_5)$	$\dot{W}_{GT,s} = \dot{m}_{CO_2}(\psi_6 - \psi_7)$
$\varepsilon_{GTHE} = \frac{\dot{m}_{exh}(\psi_{13} - \psi_{14})}{\dot{m}_{CO_2}(\psi_6 - \psi_5)}$	$\dot{E}x_{D,GT} = \dot{W}_{GT,s} - \dot{W}_{GT,a}, \varepsilon_{GT} = \frac{\dot{W}_{GT,a}}{\dot{W}_{GT,s}}$
Recuperator	**Precooler**
$\dot{m}_4 = \dot{m}_5 = \dot{m}_7 = \dot{m}_8 = \dot{m}_{CO_2}$	$\dot{m}_9 = \dot{m}_{10} = \dot{m}_{wat}, \dot{m}_1 = \dot{m}_8 = \dot{m}_{CO_2}$
$(h_4 - h_5) = (h_8 - h_7)$	$\dot{m}_{CO_2}(h_8 - h_1) = \dot{m}_{wat}(h_{10} - h_9)$
$\dot{E}x_{D,REC} = \dot{m}_{CO_2}((\psi_4 - \psi_5) - (\psi_8 - \psi_7))$	$\dot{E}x_{D,PRE} = \dot{m}_{CO_2}(\psi_8 - \psi_1) - \dot{m}_{wat}(\psi_{10} - \psi_9)$
$\varepsilon_{REC} = \frac{(\psi_4 - \psi_5)}{(\psi_8 - \psi_7)}$	$\varepsilon_{PRE} = \frac{\dot{m}_{CO_2}(\psi_8 - \psi_1)}{\dot{m}_{wat}(\psi_{10} - \psi_9)}$
Low Pressure Compressor	**High Pressure Compressor**
$\dot{m}_1 = \dot{m}_2 = \dot{m}_{CO_2}$	$\dot{m}_3 = \dot{m}_4 = \dot{m}_{CO_2}$
$\dot{W}_{LPcomp,a} = \dot{m}_{CO_2}(h_2 - h_1)$	$\dot{W}_{HPcomp,a} = \dot{m}_{CO_2}(h_4 - h_3)$
$\dot{W}_{LPcomp,s} = \dot{m}_{CO_2}(\psi_2 - \psi_1)$	$\dot{W}_{HPcomp,s} = \dot{m}_{CO_2}(\psi_4 - \psi_3)$
$\dot{E}x_{D,LPcomp} = \dot{W}_{LPcomp,a} - \dot{W}_{LPcomp,s}, \varepsilon_{LPcomp} = \frac{\dot{W}_{LPcomp,s}}{\dot{W}_{LPcomp,a}}$	$\dot{E}x_{D,HPcomp} = \dot{W}_{HPcomp,a} - \dot{W}_{HPcomp,s}, \varepsilon_{HPcomp} = \frac{\dot{W}_{HPcomp,s}}{\dot{W}_{HPcomp,a}}$
Intercooler	
$\dot{m}_{11} = \dot{m}_{12} = \dot{m}_{wat}, \dot{m}_1 = \dot{m}_8 = \dot{m}_{CO_2}$	
$\dot{m}_{CO_2}(h_2 - h_3) = \dot{m}_{wat}(h_{12} - h_{11})$	
$\dot{E}x_{D,INT} = \dot{m}_{CO_2}(\psi_2 - \psi_3) - \dot{m}_{wat}(\psi_{12} - \psi_{11})$	
$\varepsilon_{INT} = \frac{\dot{m}_{CO_2}(\psi_2 - \psi_3)}{\dot{m}_{wat}(\psi_{11} - \psi_{12})}$	

Thermoeconomics refers to the integration of exergetic analyses in the frame of economical aspect, providing engineers and operators with insights into efficiency that cannot be satisfied with traditional energy analyses and standard economical assessments. In this study, the well-known SPECO method was utilized for analyses. Initially, all energy and exergy streams throughout the system were identified. Subsequently, each subsystem was characterized in terms of the fuel–product concept. In this framework, all exergy inputs into each relevant component were treated as fuel, while the corresponding exergy outputs were regarded as the product. Following the steps of the SPECO methodology, cost balance equations together with auxiliary relations were derived for every subsystem. These formulations are summarized and presented in Table 2.

Table 2. Thermoeconomic equations-of the cycle

Gas Turbine Heat Exchanger	**Gas Turbine**
$c_{13}\dot{E}x_{13} + c_5\dot{E}x_5 + \dot{Z}_{GTHE} = c_{14}\dot{E}x_{14} + c_6\dot{E}x_6$ $c_{13} = known, \frac{\dot{C}_{13}}{\dot{E}x_{13}} = \frac{\dot{C}_{14}}{\dot{E}x_{14}}$	$c_6\dot{E}x_6 + \dot{Z}_{GT} = c_{GT}\dot{W}_{GT} + c_7\dot{E}x_7$ $\frac{\dot{C}_6}{\dot{E}x_6} = \frac{\dot{C}_7}{\dot{E}x_7}$
Recuperator	**Precooler**
$c_4\dot{E}x_4 + c_7\dot{E}x_7 + \dot{Z}_{REC} = c_5\dot{E}x_5 + c_8\dot{E}x_8$ $\frac{\dot{C}_7}{\dot{E}x_7} = \frac{\dot{C}_8}{\dot{E}x_8}$	$c_8\dot{E}x_8 + c_9\dot{E}x_9 + \dot{Z}_{PRE} = c_1\dot{E}x_1 + c_{10}\dot{E}x_{10}$ $c_9 = 0, \frac{\dot{C}_1}{\dot{E}x_1} = \frac{\dot{C}_8}{\dot{E}x_8}$
Low Pressure Compressor	**High Pressure Compressor**
$c_{LPComp}\dot{W}_{LPcomp} + \dot{Z}_{LPcomp} = c_2\dot{E}x_2 - c_1\dot{E}x_1$ $\frac{\dot{C}_1}{\dot{E}x_1} = \frac{\dot{C}_2}{\dot{E}x_2}$	$c_{HPComp}\dot{W}_{HPcomp} + \dot{Z}_{HPcomp} = c_4\dot{E}x_4 - c_3\dot{E}x_3$
Intercooler	
$c_2\dot{E}x_2 + c_{11}\dot{E}x_{11} + \dot{Z}_{INT} = c_3\dot{E}x_3 + c_{12}\dot{E}x_{12}$ $c_{11} = 0, \frac{\dot{C}_2}{\dot{E}x_2} = \frac{\dot{C}_3}{\dot{E}x_3}$	

For each system component, indicates the total cost-rate, which covers capital investment (CI), operation and maintenance (OM) contributions. The corresponding capital cost rate is calculated using the expression below [21-22]:

$$\dot{Z} = (PEC * CRF * \phi)/(3600 * N) \quad (5)$$

Table 3 represents the economic constants.

Table 3. Economic constants

Total life time(n)	*30 years*
Annual operation time (N)	*8040 hours*
Interest rate (i)	*15%*
Maintenance factor (ψ)	*1.06*
Capital recovery factor (CRF)	$RF = \frac{i(1+i)^n}{(1+i)^n - 1}$

Exergoeconomic assessments require the formulation of cost relations for individual sub-components with respect to the system's investment costs. The investment expenditures of each unit were derived from their thermodynamic parameters. Table 4 [22] provides the mathematical functions corresponding to the capital investment costs of each component.

Table 4. Purchased equipment cost functions of the cycle

Gas Turbine Heat Exchanger	$PEC_{GTHE} = 2681(A_{GTHE})^{0.59}$
Gas Turbine	$PEC_{GT} = 4405(\dot{W}_{GT})^{0.7}$
Recuperator	$PEC_{REC} = 2681(A_{REC})^{0.59}$
Precooler	$PEC_{PRE} = 2143(A_{PRE})^{0.514}$
LP and HP Compressor	$PEC_{comp} = 71.1\left[\frac{\dot{m}_{CO_2}}{0.92 - \eta_c}\right](PR)(ln(PR)$
Intercooler	$PEC_{INT} = 2143(A_{INT})^{0.514}$

All heat exchangers within the GT cycle were taken as a shell-and-tube type, and their performance was modeled using Equation (6). For this purpose, the coefficients of overall heat transfer have been taken as 1.1, 0.7, and 2 for the gas-turbine heat-exchanger, the recuperator, and both the precooler and intercooler, respectively [22].

$$\dot{Q}_k = U_k A_k LMTD$$

Furthermore, Chemical Engineering Plant Cost Index, CEPCI was employed as a vital parameter for updating the plant costs. CEPCI is evaluated as the ratio of the cost index of the reference year to that of the original year [23-25]. Since the facility commenced operation in 2011, this year was selected as the reference point. The CEPCI values for 2011 and 2025 were considered as 585.7 and 800.2, respectively, resulting in a correction factor of 0.732. Accordingly, the component costs were updated using this factor.

The performance evaluation of each subsystem was further conducted through the SPECO method. Within this framework, the exergoeconomic factor was evaluated to assess the relation between the cost flow rates and the exergy destruction associated with a component.

For a sub-component *k*, the exergoeconomic factor is expressed by Equation (7) [21].

$$f_k = \frac{\dot{Z}_k}{\dot{Z}_k + c_{f,k} \cdot \dot{E}x_{D,k}}$$

Another key indicator in thermo-economic evaluation is the relative cost difference that reflects the relative increase in an average cost per unit exergy between fuel and product of a component defining for a sub-component *k* in Equation (8) [21-22].

$$r_k = \frac{c_{p,k} - c_{f,k}}{c_{f,k}}$$

Finally, the cost-rate associated with exergy-destruction is expressed in Equation (9) [21-22].

$$\dot{D}_{D,k} = c_{f,k}\dot{E}x_{D,k}$$

3. RESULTS AND DISCUSSION

3.1. Thermodynamic and Thermoeconomic Analyses

A thermoeconomic analysis was utilized on a re-compression S-CO_2 gas-turbine cycle powered by the BSWPP exhaust gas. The thermodynamic properties of the conducted system are detailed in Table 5. T–s diagram illustrating the gas-turbine cycle is presented in Figure 3.

The thermodynamic analyses of the GT-cycle were carried out using the equations provided in Table 1, with component-specific results summarized in Table 6. The analysis revealed a net power output of 108.65 kW, energy and exergetic efficiencies of 28.02% and 53.41%, respectively. These efficiency values are consistent with those reported for other S-CO_2 gas turbine cycles in the related literature [3–15]. Nonetheless, further improvements in both energetic and exergetic efficiencies are performed by minimizing exergy destruction within the system. As indicated in Table 6, the highest and lowest exergy-destruction occurred in the gas turbine heat-exchanger and high-pressure compressor, respectively. Significant exergy-destruction in the GTHE is attributed to the use of different working fluids in heat exchangers. Conversely, the recuperator and gas turbine exhibited the highest exergy efficiencies with the relatively low exergy-destruction in the recuperator explained by the use of fluids with similar properties and phases. However, the intercooler and precooler demonstrated the lowest exergy efficiencies, which can be associated with the cooling fluids employed. Notable inefficiencies were observed because water, which differs in both phase and properties from CO_2, was selected as the working fluid for these components.

A detailed assessment of the component-level irreversibilities reveals that the intercooler, precooler, and gas turbine heat exchanger dominate the overall exergy losses of the system. To mitigate these losses within the constraints of the present model, several practical strategies can be considered. For the intercooler and precooler, the use of alternative cooling fluids—such as glycol-based mixtures, nanofluid-enhanced media, or air-cooled configurations—may improve thermal matching and reduce entropy generation. Additionally, heat transfer enhancement techniques, including corrugated plates, finned geometries, or surface augmentation, could further increase heat transfer coefficients and lower required temperature differences. For the gas turbine heat exchanger, improved flow distribution, advanced compact heat exchanger designs, or enhanced recuperative configurations may substantially decrease the large exergy destruction linked to high temperature gradients and differing fluid properties. Literature-based performance data suggest that such improvements may reduce exergy destruction in these components by approximately 10–25%, depending on the adopted enhancement method. Therefore, focusing optimization efforts on these heat exchangers is expected to yield the highest potential gains in overall system thermoeconomic performance.

Table 5. Thermodynamic properties of the related cycle

State	Fluid	T $(°C)$	P (bar)	$\dot{m}$ (kg/s)	h (kJ/kg)	s $(kJ/kg.K)$	ψ (kJ/kg)	$\dot{E}x$ (kW)
0	CO_2	20	1.0	-	-5.168	-0.01403	-	-
0'	Water	20	1.0	-	83.93	0.2962	-	-
0"	Air	20	1.0	-	293.6	5.682	-	-
1	CO_2	40	85	1.49	-128.2	-1.164	214.1	315.6
2	CO_2	70.37	139.7	1.49	-114.8	-1.164	227.8	335.8
3	CO_2	40	139.7	1.49	-218.5	-1.48	216.3	318.9
4	CO_2	52.69	229.5	1.49	-207	-1.48	228	336
5	CO_2	252.1	229.5	1.49	153.3	-0.5909	327.5	482.8
6	CO_2	411	229.5	1.49	353.7	-0.257	430.1	634.1
7	CO_2	302.1	85	1.49	237.9	-0.257	318.8	470
8	CO_2	72.69	85	1.49	-32.06	-0.8684	223.6	329.5
9	Water	20	1	2.05	84.01	0.2965	0	0
10	Water	34	1	2.05	142.5	0.4915	1.354	2.788
11	Water	20	1	5.20	84.01	0.2965	0	0
12	Water	26	1	5.20	109.1	0.3812	0.2533	1.341
13	Exhaust	431	1.9	2.18	718.1	6.398	214.7	468.2
14	Exhaust	253.2	1.9	2.18	530.5	6.092	117	255.2

Table 6. Thermodynamic results of the cycle

Component	$\dot{\boldsymbol{Q}}$ $(\boldsymbol{kW})$	$\dot{\boldsymbol{W}}$ $(\boldsymbol{kW})$	$\dot{\boldsymbol{E}}\boldsymbol{x}_{\boldsymbol{F}}$ $(\boldsymbol{kW})$	$\dot{\boldsymbol{E}}\boldsymbol{x}_{\boldsymbol{P}}$ $(\boldsymbol{kW})$	$\dot{\boldsymbol{E}}\boldsymbol{x}_{\boldsymbol{D}}$ $(\boldsymbol{kW})$	$\boldsymbol{\varepsilon}$ (%)
GTHE	347.7	-	203.5	144.5	59.02	71
GT	-	147.8	154.3	147.8	6.501	95.79
REC	531.1	-	155.2	149.4	5.759	96.29
PRE	141.8	-	13.73	2.768	10.97	20.16
LP Comp	-	21.45	21.45	18.68	2.768	87.1
HP Comp	-	17.7	17.7	15.3	2.399	86.45
INT	132.8	-	16.14	1.317	14.82	8.163
GT System	Energy efficiency (%)			28.02		
	Exergy efficiency (%)			53.41		

The related thermoeconomic performance of the GT-cycle was evaluated using SPECO method. The capital investment requirements were found using the expressions provided in Table 4, while the operating and maintenance expenses were estimated based on the CEPCI in conjunction with the expressions given in Table 3. The corresponding exergy flow rates, cost flow rates, and unit exergy costs of the GT cycle are listed in Table 7. Although the GT exhibited relatively low exergy destruction, it possessed the highest exergoeconomic factor and relative cost difference among the system components shown in Table 8. This outcome is primarily attributed to the high capital cost rate. Similarly, the GTHE is characterized by a high relative cost difference and low exergoeconomic factor because of its significant exergy destruction. Moreover, heat exchangers generally present lower exergoeconomic factor values, which result from their comparatively high exergy-destruction costs, indicating that these components require particular attention to enhance the overall system performance. In contrast, both the low- and high-pressure compressors demonstrate higher exergoeconomic factor values similar to the GT, which can be explained by their relatively low exergy destruction costs.

Table 7. Exergy flow rates, cost flow rates and unit exergy costs of the cycle

State	$\dot{E}x$ (kW)	c $(\$/GJ)$	$\dot{C}$ $(\$/h)$
1	319.3	5.008	5.757
2	338	5.008	6.094
3	321.8	5.008	5.803
4	337.1	5.02	6.093
5	492.3	5.174	9.17
6	636.8	5.008	11.48
7	482.4	5.008	8.699
8	333	5.008	6.004
9	0	0	0
10	2.768	35.22	0.351
11	0	0	0
12	1.317	82.26	0.3901
13	350.4	2.538	3.202
14	146.9	2.538	1.343

Table 8. Thermoeconomic results of the cycle

Component	$\dot{E}x_D$ (kW)	c_f $(\$/GJ)$	c_p $(\$/GJ)$	$\dot{D}_D$ $(\$/h)$	$\dot{Z}$ $(\$/h)$	r (%)	f (%)
GTHE	59.02	2.538	5.035	0.5392	0.4662	98.39	46.37
GT	6.501	5,035	8.596	0.1178	2.9210	70.72	96.12
REC	5.759	5.035	5.201	0.7202	0.3833	3.286	34.74
PRE	10.97	5.035	5.035	0.1988	0.1033	1.18 x10^{-7}	34.20
LP Comp	2.768	3.483	5.035	0.0347	0.0697	44.55	66.75
HP Comp	2.399	3.483	5.047	0.0301	0.0697	44.89	69.84
INT	14.82	5.035	5.035	0.2686	0.0991	1.22 x10^{-9}	26.96

The relationship between PEC-based capital cost functions and the exergoeconomic performance becomes particularly evident in the gas turbine. As the turbine inlet pressure increases, the PEC-based cost shows only a modest rise according to the correlations in Table 4, while the accompanying thermodynamic improvement leads to a noticeable reduction in exergy destruction. Since the GT's total cost rate combines both capital and exergy destruction costs, the net effect is a decrease in the total cost rate at higher pressures. Conversely, heat exchangers exhibit significantly higher exergy destruction, and therefore their total cost rates are primarily driven by irreversibilities rather than PEC terms, leading to low exergoeconomic factors.

3.2. Parametric Studies

The parametric studies are carried out with regarding to pressure ratio, inlet pressure of gas turbine, dead-state temperature and logarithmic mean temperature difference. Energetic and exergetic efficiencies, total net power output and total cost rate of the GT are considered with respect to limits of the variable parameters.

3.2.1. Impact of Pressure Ratio on Cycle Performance

The pressure ratio is a vital parameter for power generation systems. Consequently, in the analysis of such systems, it is customary to investigate how variations in the pressure ratio influence system outputs. As pressure ratio raises, net power output shows a consistent upward trend as shown in Figure 2. However, the energy efficiency curve demonstrates a parabolic behaviour, reaching its peak around a pressure ratio of approximately 2.4, after which efficiency slightly decreases. This indicates that there exists an optimal pressure ratio for maximizing efficiency, although higher pressure ratios continue to enhance the absolute power generation. In Figure 3, both exergy efficiency and net power output increase with higher pressure ratios, though the rate of increase in exergy efficiency diminishes beyond a PR of about 2.5. This suggests that while improvements in power generation are significant at higher pressure ratios, gains in exergy efficiency gradually saturate, indicating diminishing returns from a thermodynamic performance perspective. The total cost rate exhibits a nearly linear increasing trend as the pressure ratio rises which is given in Figure 4. This implies that operating the system at higher pressure ratios, although beneficial in terms of power generation, results in increased economic costs. Thus, a techno-economic trade-off must be considered between higher performance and elevated operating expenses.

Figure 2. Influence of PR on energetic efficiency and net power output of the cycle

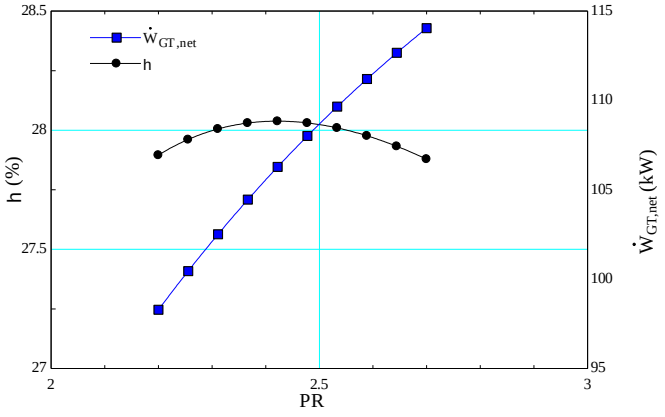

Figure 3. Influence of PR on exergetic efficiency and net power output of the cycle

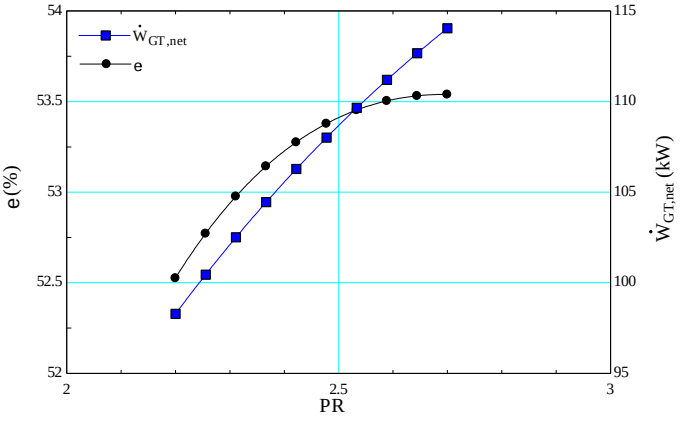

Figure 4. Influence of PR on total cost rate of the cycle

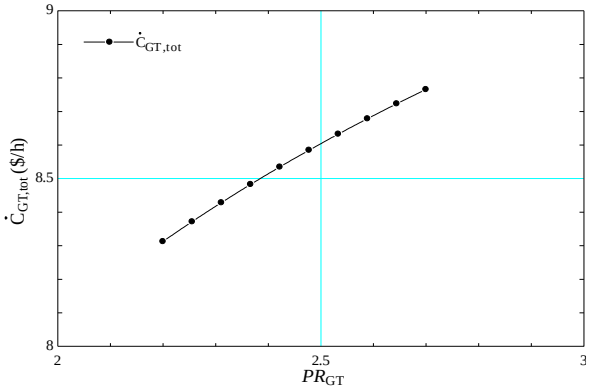

The design point selection was based on a thermo-economic compromise rather than solely maximizing net power or efficiency. Although the parametric analysis shows that net power output continues to rise with increasing pressure ratio, the cycle efficiency reaches its peak near PR = 2.5, while the total cost rate increases at higher PR values. Therefore, PR = 2.5 represents the most cost-effective operating point within the SPECO framework. Likewise, the turbine inlet pressure of approximately 229.5 bar was selected because it lies within the maximum-efficiency interval (225–230 bar) observed in the parametric analysis and ensures stable operation close to the critical region. These considerations guided the determination of the final design parameters.

3.2.2. Impact of Inlet Pressure of Gas Turbine on Cycle Performance

The effects of gas turbine inlet-pressure on power generation, energy and exergy efficiencies and total cost rate were evaluated. Figure 5 illustrates the change in energetic efficiency and net power output with respect to gas turbine inlet pressure. As the pressure rises from 185 bar to about 225 bar, both energetic efficiency and net power output rise steadily. The efficiency reaches a maximum value of approximately 28.7% near 225 bar, after which it slightly decreases, while the power output continues to increase but eventually stabilizes beyond 230 bar. This behaviour indicates that although higher inlet pressures enhance performance, there is an optimal range where efficiency gains are maximized, beyond which diminishing returns occur. The relationship between exergetic efficiency and also net power output across different turbine inlet pressures is given in Figure 6. Exergy efficiency increases gradually from around 52% to nearly 55% as pressure rises, reaching its peak in the range of 225–230 bar. The net power output follows a similar pattern, demonstrating a strong correlation with exergy efficiency. However, beyond the optimum pressure region, both parameters exhibit stabilization, and in the case of efficiency, a slight decline is observed. These results suggest that exergy utilization improves significantly with increasing pressure, but further increases beyond the optimum do not yield substantial improvements. The effect of turbine inlet pressure on the total cost-rate of the system is given in Figure 7. Unlike the efficiency trends, the total cost rate decreases consistently with increasing pressure, dropping from about 8.65 $/h at 185 bar to approximately 8.55 $/h at 235 bar. This steady reduction suggests that operating at higher inlet pressures provides a clear economic advantage, as improved thermodynamic performance translates into lower specific costs. Therefore, the results emphasize that higher gas turbine inlet pressures not only enhance technical performance but also contribute to improved economic feasibility.

Figure 5. Influence of P6 on energetic efficiency and net power output of the cycle

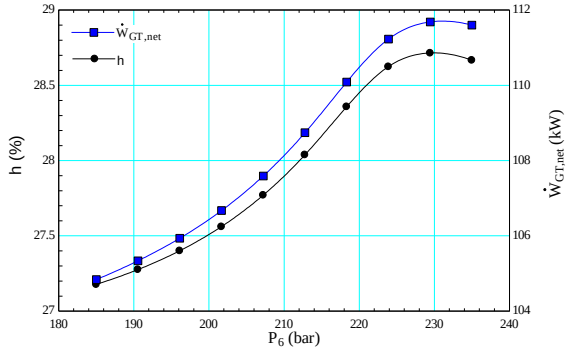

Figure 6. Influence of P6 on exergetic efficiency and net power output of the cycle

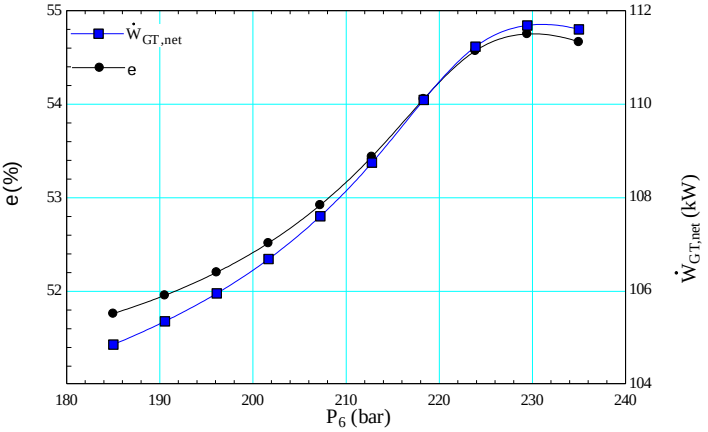

Figure 7. Influence of P6 on total cost rate of the cycle

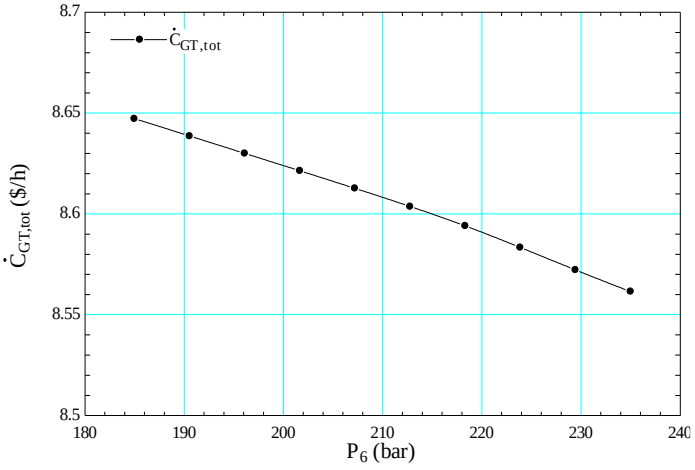

3.2.3. Impact of Dead-State Temperature on Cycle Performance

The dead-state temperature effects on thermoeconomic performance of the system were considered as another parameter. Figure 8 illustrates the change in both energetic efficiency and net power output with respect to dead-state temperature. Both parameters exhibit a clear downward trend as the temperature increases from 16 °C to 23 °C. Energetic efficiency decreases from nearly 30% to nearly 27%, while net power output drops from around 116 kW to nearly 104 kW. This indicates that higher dead state temperatures negatively affect system performance by reducing the ability of the cycle to convert available energy into useful work. Thus, operating at lower dead state temperatures enhances both efficiency and power generation. In Figure 9, the influence of dead-state temperature on both exergetic efficiency and net power output. Similar to the energy efficiency trend, both exergy efficiency and power output decline as the dead-state temperature rises. Exergy efficiency decreases from approximately 56.5% at 16 °C to about 52% at 23 °C, demonstrating the sensitivity of exergy performance to environmental reference temperature. The net power output follows the same decreasing pattern, emphasizing that increasing dead state temperature reduces the work potential and also consequently the system's effective performance. The relationship between total cost rate and dead state temperature shown in Figure 10. In contrast to efficiency trends, the total cost rate decreases steadily with increasing temperature, dropping from nearly 8.68 $/h at 16 °C to about 8.55 $/h at 23 °C. This behaviour implies that while thermodynamic performance deteriorates at higher dead state temperatures, the system's cost per unit time shows a slight economic improvement. However, considering the simultaneous drop in efficiency and power output, this economic advantage may not outweigh the performance losses, highlighting the trade-off between cost and efficiency under varying environmental conditions.

Figure 8. Influence of T0 on energetic efficiency and net power output of the cycle

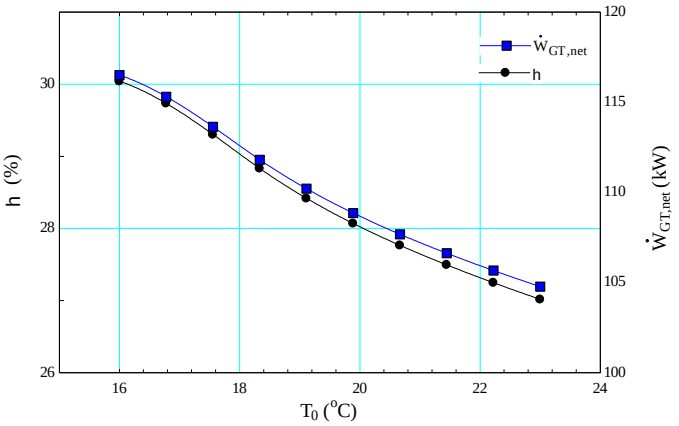

Figure 9. Influence of T0 on exergetic efficiency and net power output of the cycle

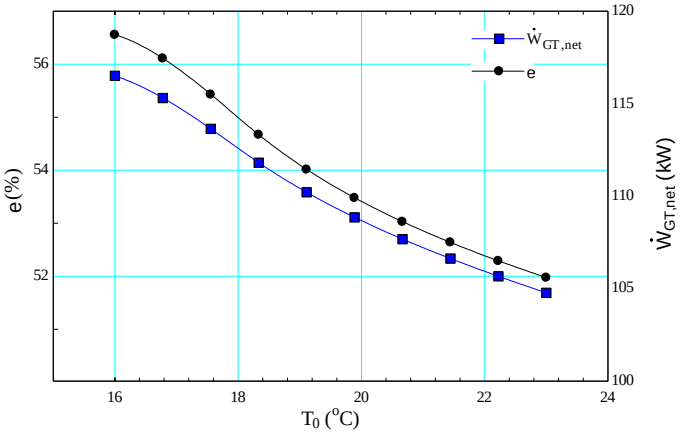

Figure 10. Influence of T0 on total cost rate of the cycle

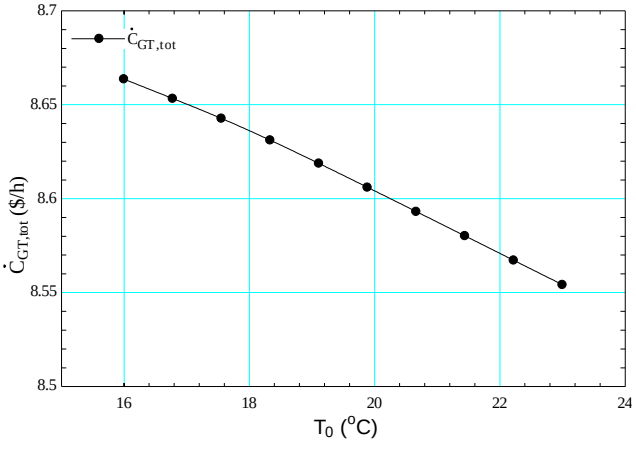

The reduction in total cost rate at higher dead-state temperatures results from the reference-state dependence of exergy. As T_0 increases, the exergy of heat and work interactions decreases, reducing exergy destruction across all components. Because exergy destruction cost dominates the SPECO cost rate while capital cost remains unchanged, the overall cost rate declines despite reductions in thermal efficiency and net power output.

3.2.4. Impact of Logarithmic Mean Temperature Difference (LMTD) on Cycle Performance

The influence of the LMTD on power generation systems is considered as another parameter to be taken into consideration. The influence of the LMTD on energetic efficiency and net power output is given in Figure 11. As LMTD increases from about 6 to 10, both efficiency and power output steadily decline. Energy efficiency drops from nearly 30% to around 26.5%, while net power output falls from nearly 112 kW to nearly 101 kW. This trend suggests that higher LMTD values reduce the thermodynamic driving force in heat exchangers, which in turn diminishes the system's energy conversion effectiveness and overall power generation. Figure 12 illustrates the variation of exergetic efficiency and also net power output with LMTD. Both parameters show a clear downward trend as LMTD increases. Exergy efficiency decreases from approximately 57% to about 50%, while net power output decreases from around 112 kW to 101 kW. The decline in exergy efficiency reflects increasing irreversibilities within the system as the temperature difference grows, leading to less effective utilization of available energy. Therefore, maintaining a lower LMTD enhances exergy performance and power output simultaneously. The relationship between total cost rate and LMTD shown in Figure 13. In contrast to efficiency trends, the total cost rate decreases only slightly as LMTD increases, dropping from about 8.62 $/h to 8.57 $/h. This indicates that the economic cost per unit time is only marginally affected by LMTD, even though efficiency and power generation are significantly reduced. Consequently, while higher LMTD values might appear economically favourable, they are not advantageous from a thermodynamic performance perspective.

Figure 11. Influence of LMTD on energetic efficiency and net power output of the cycle

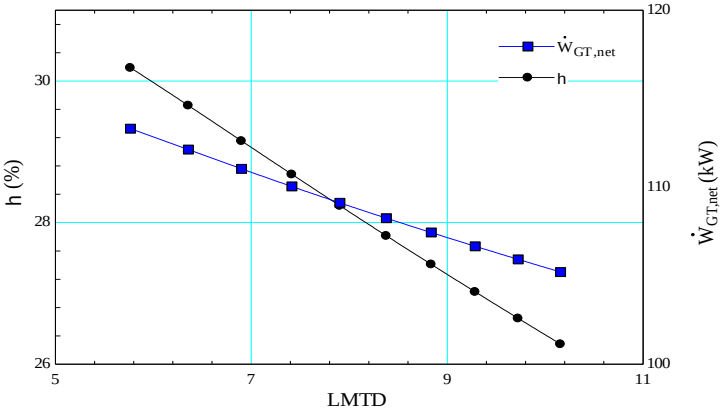

Figure 12. Influence of LMTD on exergetic efficiency and net power output of the cycle

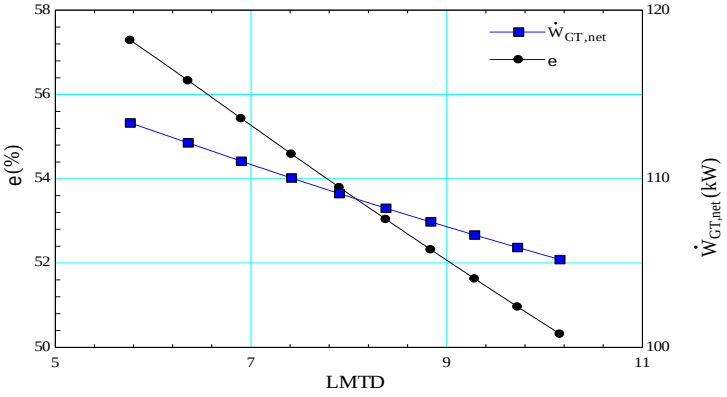

Figure 13. Influence of LMTD on total cost rate of the cycle

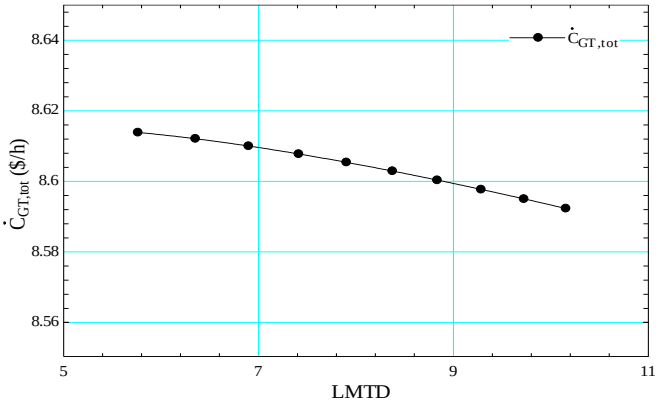

4. CONCLUSION

The thermodynamic analyses of the gas turbine (GT) system revealed that the overall energy efficiency was calculated as 28.02%, while the exergy efficiency reached 53.41%. Among the individual components, the gas turbine itself (GT) and the recuperator (REC) showed the highest exergy efficiencies, with values of 95.79% and 96.29%, respectively. In contrast, components such as the precooler (PRE) and intercooler (INT) exhibited significantly lower exergy efficiencies of 20.16% and 8.16%, which indicates substantial irreversibilities in heat exchange processes. The largest exergy-destruction occurred in the gas turbine heat exchanger (GTHE), with 59.02 kW, followed by the intercooler with 14.82 kW, highlighting the main sources of performance losses in the cycle. Herein, the highest exergy destruction amount of GTHE can be related to the difference of the temperature of the fluids and the different type phases of fluid. Besides, the high exergetic efficiencies of power producing/consuming equipments can be acceptable for all thermal power systems. It is indicated that the gas turbine heat exchanger (GTHE) and the intercooler (INT) exhibit the highest exergy-destruction values, which in turn lead to the largest cost rates of exergy-destruction within the system. The recuperator (REC), despite having relatively high thermodynamic performance, shows a considerable share of capital cost rate, making it a critical component from an investment perspective. Conversely, the compressors (LP and HP) demonstrate low unit exergy costs of fuel and product, coupled with favorable exergoeconomic factors, confirming their cost-effectiveness in the cycle. The relative cost difference (r) is most pronounced in the heat exchangers, suggesting mismatches between fuel and product costs that reduce overall system cost-effectiveness. Overall, the exergoeconomic analysis reveals that while the turbine and compressors operate efficiently in the frame of both thermodynamics and economical aspects, optimization efforts should primarily focus on the heat exchangers, especially the GTHE and INT, to minimize cost-based irreversibilities and enhance the economic sustainability of the cycle. This outcome is consistent with the expected behaviour of heat exchangers. Based on these results, future studies should focus on developing the thermodynamic and economic performance of heat exchangers, particularly the gas turbine heat-exchanger and the intercooler, as they contribute most to exergy destruction and cost irreversibilities. Advanced heat transfer enhancement techniques, alternative working fluids, or novel exchanger configurations may be investigated to reduce losses and improve exergoeconomic factors. In addition, system-level optimization approaches, such as multi objective optimization considering both efficiency and cost, could be applied to identify more sustainable operating conditions. Finally, integrating the cycle with other heat recovery systems or renewable energy sources may further enhance overall system efficiency and economical viability, making the configuration more attractive for real-world applications.

Nomenclature

A	heat transfer area, m^2
$\dot{C}$	cost rate, \$/h
c	cost per exergy unit, \$/GJ
c_f	unit exergy cost of fuel, \$/GJ
c_p	unit exergy cost of fuel, \$/GJ
$\dot{D}$	cost rate of exergy destruction, \$/h
$\dot{E}x$	exergy rate, kW
f	exergoeconomic factor
h	specific enthalpy, kJ/kg
i	interest rate
$\dot{m}$	mass flow rate, kg/s
n	total life time
N	annual operation time
P	pressure, bar
PR	pressure ratio
$\dot{Q}$	heat addition, kW
r	relative cost difference
s	specific entropy, kJ/kg-K
T	temperature, ^oC
U	heat transfer coefficient, kW/m^2-K
$\dot{W}$	work flow rate-power, kW
$\dot{Z}$	capital cost rate, \$/h

Greek symbols

ε	exergy efficiency
εf	effectiveness
η	energy efficiency
η_C	compressor isentropic efficiency
η_{GT}	turbine isentropic efficiency
ϕ	maintenance factor
ψ	specific flow exergy, kJ/kg

Subscripts

0	dead state
a	actual
crit	critical point
D	destruction
exh	exhaust
k	component
s	isentropic
tot	total
wat	water

Abbreviations

CEPCI	chemical engineering plant cost index
CRF	capital recovery factor
EMO	evolutionary multi-objective optimization
GMSWPP	Gaziantep Municipal Solid Waste Power Plant
GT	gas turbine
GTHE	gas turbine heat exchanger
HE	heat exchanger
HP Comp	high pressure compressor
INT	intercooler
LMTD	logarithmic mean temperature difference
LP Comp	low pressure compressor
NSGA-II	non-dominated sorting genetic algorithm
PEC	purchased equipment cost
PRE	precooler
REC	recuperator
S-CO_2	supercritical carbon dioxide
SPECO	specific exergy costing
T-CO_2	transcritical carbon dioxide

Acknowledgements

This study is supported by TUBİTAK (the Scientific and Technological Research Council of Turkey) with the project under the grant number of 114M142. The authors would like to thank TUBİTAK and CEV (Clean Energy & Vehicles) energy.

REFERENCES

[1] O. Olumayegun, M. Wang, and G. Kelsall, "Closed-cycle gas turbine for power generation: A state-of-the-art review," *Fuel*, vol. 180, pp. 694–717, 2016.

[2] Reuters Echogen Power Systems, "Waste heat recovery system available as turnkey solution 1," 2014–2015.

[3] Y. Ahn, S. Bae, M. Kim, S. Cho, S. Baik, J. Lee, and J. E. Cha, "Review of supercritical CO2 power cycle technology and current status of research and development," *Nucl. Eng. Technol.*, vol. 47, pp. 647–661, 2015.

[4] A. D. Akbari and S. M. S. Mahmoudi, "Thermoeconomic analysis & optimization of the combined supercritical CO2 recompression Brayton/organic Rankine cycle," *Energy*, vol. 78, pp. 501–512, 2014.

[5] J. Cha, T. Lee, J. Eoh, S. Seong, S. Kim, D. Kim, M. H. Kim, T.-W. Kim, and K.-Y. Suh, "Development of a supercritical CO2 Brayton energy conversion system coupled with a sodium cooled fast reactor," *Nucl. Eng. Technol.*, vol. 41, pp. 1025–1044, 2009.

[6] S. Ishiyama, Y. Muto, Y. Kato, S. Nishio, T. Hayashi, and Y. Nomoto, "Study of steam, helium and supercritical CO2 turbine power generations in prototype fusion power reactor," *Prog. Nucl. Energy*, vol. 50, pp. 325–332, 2008.

[7] F. Mohammadkhani, N. Shokati, S. M. S. Mahmoudi, M. Yari, and M. A. Rosen, "Exergoeconomic assessment and parametric study of a gas turbine-modular helium reactor combined with two organic Rankine cycles," *Energy*, vol. 65, pp. 533–543, 2014.

[8] X. Wang and Y. Dai, "An exergoeconomic assessment of waste heat recovery from a Gas Turbine-Modular Helium Reactor using two transcritical CO2 cycles," *Energy Convers. Manage.*, vol. 126, pp. 561–572, 2016.

[9] J. Wang, Z. Yan, M. Wang, M. Li, and Y. Dai, "Multi-objective optimization of an organic Rankine cycle (ORC) for low grade waste heat recovery using evolutionary algorithm," *Energy Convers. Manage.*, vol. 71, pp. 146–158, 2013.

[10] J. Wang, Z. Sun, Y. Dai, and S. Ma, "Parametric optimization design for supercritical CO2 power cycle using genetic algorithm and artificial neural network," *Appl. Energy*, vol. 87, pp. 1317–1324, 2010.

[11] A. Kouta, A. F. Al-Sulaiman, and M. Atif, "Energy analysis of a solar driven cogeneration system using supercritical CO2 power cycle and MEE-TVC desalination system," *Energy*, vol. 119, pp. 996–1009, 2017.

[12] D. Milani, M. Tri Luu, R. McNaughton, and A. Abbas, "A comparative study of solar heliostat assisted supercritical CO2 recompression Brayton cycles: dynamic modelling and control strategies," *J. Supercrit. Fluids*, vol. 120, pp. 113–124, 2017.

[13] H. Nami, S. M. S. Mahmoudi, and A. Nemati, "Exergy, economic and environmental impact assessment and optimization of a novel cogeneration system including a gas turbine, a supercritical CO2 and an organic Rankine cycle (GT-HRSG/SCO2)," *Appl. Therm. Eng.*, vol. 110, pp. 1315–1330, 2017.

[14] M. H. Ahmadi, M. Mehrpooya, and F. Pourfayaz, "Exergoeconomic analysis and multi objective optimization of performance of a Carbon dioxide power cycle driven by geothermal energy with liquefied natural gas as its heat sink," *Energy Convers. Manage.*, vol. 119, pp. 422–434, 2016.

[15] M. S. Kim, Y. Ahn, B. Kim, and J. I. Lee, "Study on the supercritical CO2 power cycles for landfill gas firing gas turbine bottoming cycle," *Energy*, vol. 111, pp. 893–909, 2016.

[16] F. A. Boyaghchi and H. Safari, "Parametric study and multi-criteria optimization of total exergetic and cost rates improvement potentials of a new geothermal based quadruple energy system," *Energy Convers. Manage.*, vol. 137, pp. 130–141, 2017.

[17] Y. Feng, Y. Zhang, B. Li, J. Yang, and Y. Shi, "Comparison between regenerative organic Rankine cycle (RORC) and basic organic Rankine cycle (BORC) based on thermoeconomic multi-objective optimization considering exergy efficiency and levelized energy cost (LEC)," *Energy Convers. Manage.*, vol. 96, pp. 58–71, 2015.

[18] Z. Hajabdollahi and P. F. Fu, "Multi-objective-based configuration optimization of SOFC-GT cogeneration plant," *Appl. Therm. Eng.*, vol. 112, pp. 549–559, 2017.

[19] V. Jain, G. Sachdeva, S. S. Kachhwaha, and B. Patel, "Thermo-economic and environmental analyses based multi-objective optimization of vapor compression absorption cascaded refrigeration system using NSGA-II technique," *Energy Convers. Manage.*, vol. 113, pp. 230–242, 2016.

[20] Y. Li, S. Liao, and G. Liu, "Thermo-economic multi-objective optimization for a solardish Brayton system using NSGA-II and decision making," *Electr. Power Energy Syst.*, vol. 64, pp. 167–175, 2015.

[21] O. Güngör, A. Tozlu, C. Arslantürk, and E. Özahi, "District heating based on exhaust gas produced from end-of-life tires in Erzincan: Thermoeconomic analysis and optimization," *Energy*, vol. 294, p. 130755, 2024.

[22] A. Tozlu, E. Özahi, and A. Abuşoğlu, "Waste to Energy Technologies for Municipal Solid Waste Management in Gaziantep," *Renew. Sustain. Energy Rev.*, vol. 54, pp. 809–815, 2016.

[23] A. Tozlu, E. Özahi, and A. Abuşoğlu, "Energetic and Exergetic Analyses of a Solid Waste Power Plant using Aspen Plus," *Int. J. Energy*, vol. 10, pp. 44–47, 2016.

[24] V. Zare, S. M. S. Mahmoudi, and M. Yari, "An exergoeconomic investigation of waste heat recovery from the Gas Turbine-Modular Helium Reactor (GT-MHR) employing an ammonia-water power/cooling cycle," *Energy*, vol. 61, pp. 397–409, 2013.

[25] H. Ozcan and I. Dincer, "Exergoeconomic optimization of a new four-step magnesium chlorine cycle," *Int. J. Hydrogen Energy*, vol. 42, pp. 2435–2445, 2017.